Macromolecular Research, Vol. 17, No. 12, pp 976-986 (2009)

The Alignment of Liquid Crystals on the Film Surfaces of Soluble Aromatic Polyimides Bearing *t*-Butylphenyl and Trimethylsilylphenyl Side Groups

Suk Gyu Hahm†, Kyeong Sik Jin, Samdae Park, and Moonhor Ree*

Department of Chemistry, Pohang Accelerator Laboratory, National Research Laboratory for Polymer Synthesis and Physics, Center for Electro-Photo Behaviors in Advanced Molecular Systems, BK School of Molecular Science, Division of Advanced Materials Science, and Polymer Research Institute, Pohang University of Science & Technology, Pohang 790-784, Korea

Hyung-Sun Kim† and Soon-Ki Kwon*

School of Materials Science and Engineering and Engineering Research Institute, Gyeongsang National University, Jinju 660-701, Korea

Yun-Hi Kim

Department of Chemistry & RINS, Gyeongsang National University, Jinju 660-701, Korea

Received April 7, 2009; Revised May 30, 2009; Accepted June 1, 2009

Abstract: With the study goal of firstly elucidating the anisotropic interactions between oriented polymer chain segments and liquid crystal (LC) molecules, and secondly of determining the contributions of the chemical components of the polymer segments to the film surface topography, LC alignment, pretilt, and anchoring energy, we synthesized three dianhydrides, 1,4-bis(4'-*t*-butylphenyl)pyromellitic dianhydride (BBPD), 1,4-bis(4'-trimethylsilylphenyl)pyromellitic dianhydride (BTPD), and 2,2'-bis(4''-*tert*-butylphenyl)-4,4',5,5'-biphenyltetracarboxylic dianhydride (BBBPAn), and a series of their organosoluble polyimides, BBPD-ODA, BBPD-MDA, BBPD-FDA, BTPD-FDA, and BBBPAn-FDA, which contain the diamines 4,4'-oxydianiline (ODA), 4,4'-methylenediamine (MDA), and 4,4'-(hexafluoroisopropylidene)dianiline (FDA). All the polyimides were determined to be positive birefringent polymers, regardless of the chemical components. Although all the rubbed polyimide films exhibited microgrooves which were created by rubbing process, the film surface topography varied depending on the polyimides. In all the rubbed films, the polymer chains were unidirectionally oriented along the rubbing direction. However, the degree of in-plane birefringence in the rubbed film varied depending on the polyimides. The rubbing-aligned polymer chains in the polyimide films effectively induced the alignment of nematic LCs along their orientation directors by anisotropic interactions between the preferentially oriented polymer chain segments and the LCs. The azimuthal and polar anchoring energies of the LCs ranged from 0.45×10^{-4} - 1.37×10^{-4} J/m^2 and from 0.86×10^{-5} - 4.26×10^{-5} J/m^2, respectively, depending on the polyimides. The pretilt angles of the LCs were in the range 0.10-0.62°. In summary, the soluble aromatic polyimides reported here are promising LC alignment layer candidates for the production of advanced LC display devices.

Keywords: aromatic polyimides, nanoscale thin films, liquid crystals, rubbing process, surface chain orientation, surface topography, microgrooves, anisotropic molecular interaction, liquid crystal orientation, optical retardation, azimuthal anchoring energy, polar anchoring energy.

Introduction

Polyimides (PIs) have high glass transition temperatures, dimensional stability, and heat resistance as well as excellent mechanical and dielectric properties, optical transparency, and adhesion.[1-45] One of the most recently developed applications of PIs is their use as liquid crystal (LC) alignment layers in flat-panel LC display (LCD) devices.[46-72] LC alignment PI layers are known to stably anchor LC molecules, which is critical to the high performance and reliability of LCD devices.[46-72] PI film surfaces need to be treated if they are to produce the uniform alignment of LC molecules with a defined range of pretilt angle values.[46-72] Rubbing with a velvet fabric is currently the only technique used to treat PI film surfaces in the mass-production of flat-panel LCD devices by the LCD industry. This process has become

*Corresponding Authors. E-mails: ree@postech.edu or skwon@gnu.ac.kr

†S. G. Hahm and H.-S. Kim contributed equally to this work.

the method of choice because of its simplicity and the controllability with this method of both the LC anchoring energy and the pretilt angle.[46-68]

The rubbing process is known to modify the surface morphology and to orient the polymer chains in the alignment layer film.[46-68] It is therefore not only important to examine the modification of the film surface produced by rubbing, but also to understand the mechanism of rubbing-induced molecular orientation. These issues have been examined in a variety of studies.[55,73-76] Atomic force microscopy (AFM) has been used to study rubbed film surfaces.[55] These studies showed that as the rubbing depth (density) increases, microgrooves are produced that are aligned parallel or perpendicularly to the rubbing direction. The anisotropic alignment of the polymer chains has been examined with optical phase retardation measurements,[55] second harmonic generation,[73] near edge X-ray absorption spectroscopy,[74] grazing incident X-ray scattering,[75] and polarized infrared spectroscopy.[55,76] These methods provide information about the surface topographies of rubbed polymer films, as well as about the molecular orientations within the films and the thickness of the oriented layers. However, the critical information required for understanding the effects of rubbing the surfaces of films is a characterization of the events involved in the orientation of polymer chains in the rubbed films, and these events have yet to be investigated in detail.

Much effort has also been exerted in the investigation of the mechanism behind the alignment of LC molecules on rubbed PI surfaces over the last ten years. A variety of factors has been proposed to explain the surface anchoring and alignment of LC molecules: (i) microgrooves in connection with anisotropic LC orientational elasticity via steric interactions,[77-86] (ii) polymer molecules from the velvet fabric deposited and oriented on the alignment layer surface during the rubbing process,[67,87,88] (iii) anisotropically oriented polymer chains,[43-66,74,75,88-105] (iv) a near-surface order parameter different from that of bulk LC molecules,[105,106] (v) surface electric fields,[107] and (vi) coupling of the bending mode of the LC director with surface electric fields.[108] Of the mechanisms proposed so far, the anisotropic polymer chain orientation mechanism[43-66,74,75,88-105] and the microgroove mechanism[77-86] are widely accepted. Nevertheless, the anisotropic polymer chain orientation and microgroove mechanisms are still the subjects of debate in aspects of understanding their quantitative contributions to the LC alignment on rubbed polymer film surfaces. Further, the processes determining the pretilt angle of LC molecules on polymer film surfaces have rarely been investigated.

In this study, we synthesized the interesting chemical structures of three dianhydrides, 1,4-bis(4'-*t*-butylphenyl) pyromellitic dianhydride (BBPD), 1,4-bis(4'-trimethylsilylphenyl) pyromellitic dianhydride (BTPD), and 2,2'-bis(4"-*tert*-butylphenyl)-4,4',5,5'-biphenyltetracarboxylic dianhydride (BBBPAn), and a series of their organosoluble polyimides BBPD-ODA, BBPD-MDA, BBPD-FDA, BTPD-FDA, and BBBPAn-FDA containing the diamines 4,4'-oxydianiline (ODA), 4,4'-methylenediamine (MDA), and 4,4'-(hexafluoroisopropylidene)dianiline (FDA) in order to investigate the contribution of the dianhydride units to anchor and align LC molecules at the polyimide film surface. To determine the orientations of the polyimide chains produced at various rubbing strengths, the surface orientational distributions of the main chains of the corresponding PIs were measured by using optical retardation analysis and the surface topographies of the PI films were examined with AFM. The alignments of LC molecules in contact with the rubbed PI films were investigated and, furthermore, the pretilt behaviors and anchoring energies of the LCs on the PI films were determined. The measured LC alignment, pretilt, and anchoring characteristics were analyzed to elucidate the anisotropic interactions between the oriented polymer chain segments and the LC molecules. In addition, the contributions in each case of the chemical components of the polymer segments to the film surface topography, the LC alignment, pretilt, and the anchoring energy were determined.

Experimental

Materials and Film Preparation. The three dianhydrides, 1,4-bis(4'-*t*-butylphenyl)pyromellitic dianhydride (BBPD), 1,4-bis(4'-trimethylsilylphenyl)pyromellitic dianhydride (BTPD), and 2,2'-bis(4"-*tert*-butylphenyl)-4,4',5,5'-biphenyltetracarboxylic dianhydride (BBBPAn) were prepared and a series of their organosoluble polyimides [BBPD-ODA, BBPD-MDA, BBPD-FDA, BTPD-FDA, and BBBPAn-FDA (Figure 1)] were synthesized from the obtained dianhydrides and respective aromatic diamines by the conventional polycondensation reaction followed by high-temperature, one-step polymerization, according to the method described previously.[109,110] Diamines, 4,4'-oxydianiline (ODA), 4,4'-(hexafluoroisopropylidene)dianiline (FDA), and methylenedianiline (MDA) were purchased from Aldrich Chemical Company and used as received.

Each PI solution was diluted to 2% (w/v) with dried chloroform and then the diluted chloroform solution was spin-coated onto silicone substrates for AFM images, and indium tin oxide (ITO) glass substrates for optical retardations and LC cell assemblies, followed by drying on a hot plate at 80 °C for 1 h. The dried PI films were measured to have a thickness of around 100 nm, using a spectroscopic ellipsometer (model M2000, J. A. Woollam) and an α-stepper (model Tektak3, Veeco). The PI films coated onto the substrates were rubbed at various rubbing strengths using a laboratory rubbing machine (Wande) with a roller covered with a rayon velvet fabric (model YA-20-R, Yoshikawa, Japan). The rubbing strength was varied by changing the cumulative rubbing time for a constant rubbing depth, 0.25 mm.

LC Cell Preparation. Some of the rubbed PI films on

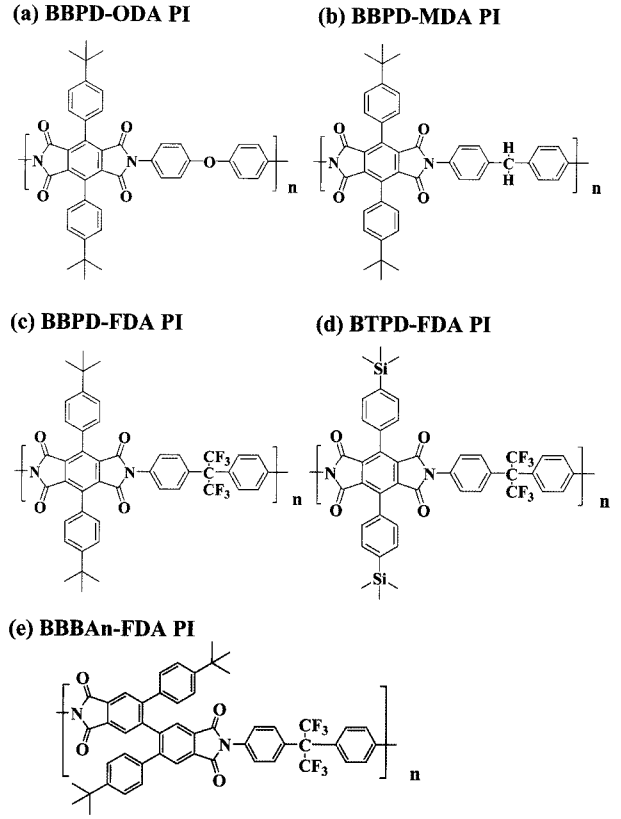

Figure 1. Chemical structures of the soluble aromatic polyimides containing *t*-butylphenyl and trimethylsilylphenyl side groups.

glass substrates were cut into 2.5 cm×2.5 cm pieces and then used for assembling two different LC cells as follows. First, paired pieces cut from each glass substrate were assembled together antiparallel with respect to the rubbing direction by using 50 μm thick spacers, injected with a nematic LC, 4-*n*-pentyl-4'-cyanobiphenyl (5CB) (n_e(extraordinary refractive index)=1.717 and n_o(ordinary refractive index)=1.53) containing 1.0 wt% Disperse Blue 1 as a dichroic dye, and then sealed with an epoxy glue, giving antiparallel nematic LC cells. Secondly, paired pieces from each glass substrate were assembled together orthogonal to the rubbing direction by using silica balls of 4.0 μm diameter as spacers, injected with the LC and then sealed with an epoxy glue, giving 90°-twisted nematic LC cells (TN LC cells). All the prepared LC cells were found to be uniform and homogeneous throughout by optical microscopy. Third, paired pieces from the same ITO glass substrate were assembled together by using silica balls with a diameter of 50 μm as spacers, aligning the direction antiparallel to the rubbing direction and 5CB LC molecules were injected into the cell gap, followed by sealing of the injection hole with a commercialized sealant minimizing ion-induced space charge, giving antiparallel nematic LC cells with the rubbed films, respectively. Leads were attached to the cell so that electric field can be applicable and go through the LC layer thickness direction.

Measurements. Thermogravimetric analysis (TGA) was performed under nitrogen on a TA instruments 2050 thermogravimetric analyzer. The sample was heated with a heating rate of 10 °C/min from 50 to 800 °C. Differential scanning calorimetry (DSC) was conducted under nitrogen on a TA instruments 2100 differential scanning calorimeter. The sample was heated with a heating rate of 10 °C/min from 30 to 400 °C. Inherent viscosities were measured in chloroform solution (0.5 g/dL) at 25 °C using a Canon Fenske viscometer.

The dried powder samples were characterized by wide-angle X-ray diffraction (WAXD). WAXD measurements were performed using a Rigaku diffractometer (Model Rint-2000) with a vertical type goniometer and a rotating anode X-ray generator. The entire system was automated by software running in a Unix environment on an HP workstation. All measurements were carried out in $\theta/2\theta$ mode in the reflection geometry. The Ni-filtered CuK_α radiation source was operated at 40 kV and 60 mA. The 2θ scan data were collected in a fixed time mode (3 s) with step size of 0.05° over the range 1.5-25°.

The surface morphology of the PI films was measured before and after rubbing, using an atomic force microscope (Digital Instruments, model Multimode AFM Nanoscope IIIa) in contact mode. The film surface was scanned using an ultralever cantilever (with a 26 N/m spring constant and 268 kHz resonance frequency). Image processing and data analysis were performed using a software program provided by Digital Instruments. Optical phase retardations were measured using an optical set up equipped with either a photoelastic modulator (model PEM90, Hinds Instruments) with a fused silica head or a quarter plate (Oriel). The optical phase retardation measurements were calibrated with a $\lambda/30$ plate standard (Wave plate zero order $\lambda/30$ (λ=632.8 nm), Altechna); λ is the wavelength of a laser light source. Samples were installed perpendicular to the incident beam direction. Optical phase retardations were measured as a function of the angle of rotation of the samples.

The LC alignment of antiparallel LC cells was examined using an optical setup that was equipped with a He-Ne laser (632.8 nm wavelength), a polarizer, a photodiode detector, and a goniometer. In the measurement, the laser beam was incident perpendicular to the surface of the LC cell mounted on the goniometer, and these components were placed between the polarizer and the detector. Light absorption of the dichroic dye aligned together with the LC molecules in the cell was then monitored as a function of the angle of rotation of the cell. The pretilt angle α of the LC molecules was measured using a crystal rotation apparatus.[52-55,69-71,89-96]

For the TN LC cells, azimuthal anchoring energy was measured by using an ultraviolet-visible (UV-vis) spectrophotometer (model S-300, Scinco, Korea) equipped with two Glan-Laser prisms (model PGL5015, Casix, China);

the analyzer was mounted on a motorized goniometer (model SKIDS-PH, Sigma Koki, Japan). Each TN cell was placed between the polarizer and the analyzer. UV-vis spectra were recorded at 0.8 cm^{-1} resolution as a function of the angle of rotation of the analyzer in the range 0-180° with an interval of 1.0°. In these measurements, the rotation angles giving a minimum transmittance in the UV-vis spectra were determined. Of the rotation angles for which measurements were carried out, one angle was chosen by considering the nature of the birefringence dispersion of the LC and used for determining the twist angle at which the easy axes of the upper and lower substrates of the cell occur.[52-55,69-71,89-96] The azimuthal anchoring energies of the LCs on the rubbed PI film surfaces were estimated from the twist angle using the optical parameters of the LC.[52,69-71,95,96]

For the measurement of polar anchoring energy, we adopted the resistance-voltage technique[111,112] where one measures only the retardation of the cell as a function of applied voltage. No capacitance measurements are needed to determine anchoring energy when the dielectric constant of the liquid crystal is known. First, the optical phase retardation of the LC cell under the application of electric field was determined by the Senarmont technique.[113,114] In this method, optical elements are a He-Ne laser of 632.8 nm wavelength (Spectra-Physics, model 106-1) as a light source, a pair of polarizers (Oriel, model 27300), a photodiode detector (UDT Sensors, model PIN-10DL), and a quarter-wave plate (Newport optics, model 59260) with optical-wave plate. The second polarizer as an analyzer was set up mounted on a motorized goniometer (model SKIDS-PH, Sigma Koki, Tokyo, Japan) and rotated into the crossed position with the first polarizer. Each optical element arranged in a row was placed perpendicular to the laser direction and experimental setup to measure is like described elsewhere.[111,112] The applied voltage was controlled from 0 to 20 V using an Agilent 4284A precision LCR meter. All measurements were conducted at room temperature and the temperature change of the cell due to a high applied voltage (up to 20 V) was determined to be negligible.

Results and Discussion

High molecular weight polyimides were successfully synthesized and found to have high inherent viscosities (η_{inh}) in the range 0.41-1.98 dL/g: 1.98 dL/g for BBPD-ODA, 0.64 dL/g for BBPD-MDA, 0.62 dL/g for BBPD-FDA, 1.06 dL/g for BTPD-FDA, and 0.41 dL/g for BBBPAn-FDA. The thermal properties of the polyimides were investigated by carrying out DSC and TGA in a nitrogen atmosphere. The TGA results show that the BBBPAn-FDA polyimide exhibits thermal stability up to 549 °C; the other polymers were found to be stable up to 500-510 °C. The glass transition temperatures (T_g) of the polyimides were found to be 381 °C for BBBPAn-FDA, 292.3 °C for BBPD-ODA, 291.7 °C for BBPD-MDA, 259.6 °C for BBPD-FDA, and 245.6 °C for BTPD-FDA.

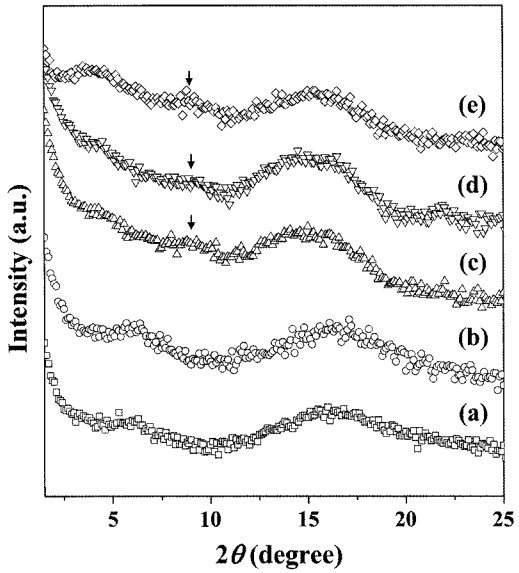

Figure 2. WAXD patterns of the polyimides: (a) BBPD-ODA PI; (b) BBPD-MDA PI; (c) BBPD-FDA PI; (d) BTPD-FDA PI; (e) BBBAn-FDA PI. The arrows indicate the second order diffractions.

WAXD Measurements. Figure 2 shows the WAXD patterns of the PI samples. For both the BBPD-ODA and BBPD-MDA PIs, the WAXD patterns contain two diffraction peaks in the range 3-25° (2θ). According to the peaks at higher angles spreading from 10 to 25° (2θ), the d-spacing values are 5.5 Å for the BBPD-ODA PI and 5.3 Å for the BBPD-MDA PI. These d-spacing values might be due to the mean value of the polymer-polymer interchain distance. The d-spacing values estimated from the peaks at lower angles spreading over the range 3-10° are 15.4 Å for the BBPD-ODA PI and 14.7 Å for the BBPD-MDA PI. These peaks might be related to the average intra-distance of the repeated units of the respective polymer single chains. Taking this into account, the determined d-spacing values are a barometer to reflect the polymer chain rigidity. In comparison, the d-spacing value of the BBPD-ODA PI is slightly larger than that of the BBPD-MDA PI. However, the ether linker is generally known to be flexible compared to the hydrocarbon linker. Due to this flexible ether linker, the BBPD-ODA PI is expected to reveal slightly lower polymer chain rigidity than that of the BBPD-MDA PI.

For the BBPD-FDA, BTPD-FDA, and BBBAn-FDA PIs, each WAXD pattern contains three peaks in the range 2-20° (Figure 2). Two weak diffraction peaks are present in each of these patterns in the range 2-11°, with one diffraction peak in the range 11-20°. According to the peaks at higher angles spreading from 11 to 20° (2θ), the d-spacing values are 5.9 Å for the BBPD-FDA PI, 5.8 Å for the BTPD-FDA PI, and 5.7 Å for the BBBAn-FDA PI. These d-spacing

Table I. The *d*-Spacing Values of Various Polyimides (PIs) Determined from the First Diffraction in the Small Angle Region and from the Wide Angle Diffraction

Polymer	Small Angle Region	Wide Angle Region
	d-Spacing (Å)	*d*-Spacing (Å)
BBPD-ODA PI	15.3	5.5
BBPD-MDA PI	14.6	5.2
BBPD-FDA PI	19.8	5.9
BTPD-FDA PI	19.3	5.8
BBBAn-FDA PI	21.5	5.7

values might correspond to the mean value of the polymer-polymer interchain distance. On the other hand, the *d*-spacing values estimated from the peaks at lower angles spreading over the range 2-11° are 19.8 Å for the BBPD-FDA PI, 19.3 Å for the BTPD-FDA PI, and 21.5 Å for the BBBAn-FDA PI. These peaks might be related to the average intra-distance of the repeated units of the respective polymer single chains.

As summarized in Table I, the diffraction peaks of the BBPD-FDA, BTPD-FDA, and BBBAn-FDA PIs are slightly shifted to the lower angle region with respect to those of the BBPD-ODA and BBPD-MDA PIs and their average *d*-spacing values are correspondingly higher. This phenomenon is apparently caused by the enhanced rigidity of the polymer chains that results from the introduction of the bulky trifluoromethyl substituents, which reduces space-efficient packing in a constitutive manner. In addition, the highest value of those PIs with FDA units arises for the BBBAn-FDA PI, which reflects the bulkiness of the twisted biphenyl groups in the polymer chains.

Surface Morphology. By using AFM, we examined the surfaces of the PI films in detail before and after they had been rubbed with various rubbing strengths. Figure 3(a) shows an AFM image of unrubbed BTPD-FDA. The BTPD-FDA film was found to have a root-mean-square (rms) roughness of 0.36 nm over an area of $1.0 \times 1.0\ \mu m^2$. The other unrubbed PI films were also found to have an rms roughness of 0.36 nm over an area of $1.0 \times 1.0\ \mu m^2$ (images not shown). Figures 3(b)~(e) show representative AFM images of the PI films after rubbing at a rubbing strength of 120 cm.

As can be seen in Figure 3(b), the surface of the BBPD-ODA film rubbed with a rubbing strength of 120 cm contains microgrooves that run parallel to the rubbing direction, which resemble those reported for rubbed films of conventional PIs used in the LCD industry.[43,44,115-117] The rms surface roughness of this rubbed PI film is 1.62 nm, which is higher than that of the unrubbed film. The width of the grooves in the surface is 84 nm and the depth between grooves is 3.99 nm. Figure 3(c) shows a representative AFM image of the BBPD-MDA films rubbed with a rubbing strength of 120 cm. As can be seen in the figure, the surface of this rubbed PI film also contains microgrooves that run parallel to the rubbing direction, with an rms surface roughness of 2.66 nm. The height of the grooves running parallel to the rubbing direction is 10.26 nm and the width of the valleys around the grooves is 117.19 nm.

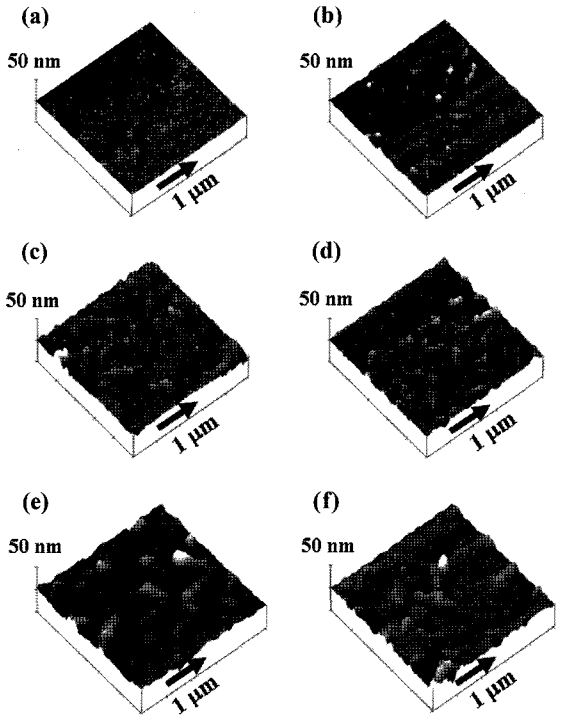

Figure 3. Surface AFM images of the PI films before and after rubbing at a rubbing strength of 120 cm: (a) unrubbed BTPD-FDA PI; (b) rubbed BBPD-ODA PI; (c) rubbed BBPD-MDA PI; (d) rubbed BBPD-FDA PI; (e) rubbed BTPD-FDA PI; (f) rubbed BBBAn-FDA PI. The arrows in these AFM images indicate the rubbing direction.

Figure 3(d) shows a representative AFM image of BBPD-FDA PI films rubbed at a rubbing strength of 120 cm. As can be seen in this figure, the rubbed PI film has an rms surface roughness of 2.46 nm. Unlike the two AFM images discussed above, microgrooves running parallel to the rubbing direction are difficult to discern, but submicroscale grooves run perpendicular to the rubbing direction that significantly increase the surface rms roughness. As can be seen in Figure 3(e), the rubbed BTPD-FDA PI film has an rms surface roughness of 4.48 nm, and contains submicroscale grooves that lie perpendicular to the rubbing. The average height and width of the submicroscale grooves are 13.86 and 103.52 nm respectively. The rubbed BBBPAn-FDA PI film has an rms surface roughness of 3.90 nm, and has submicroscale grooves that lie perpendicular to the rubbing direction and contribute significantly to the surface rms roughness (Figure 3(f)).

The differences between the observed surface morphologies might be due to the differences between the character-

istic deformation responses of the PIs to the shear force caused by the contact of fibers with the surfaces during the rubbing process. In fact, it is very hard to find correlations of the observed surface topographies in the rubbed PI films to the PIs' chemical and physical natures. However, some correlations can be considered as follows. First, the relatively less rigid BBPD-ODA and BBPD-MDA PIs in films reveal microgrooves parallel aligned along the rubbing direction, while the more rigid PIs containing trifluoromethyl groups in films show microgrooves perpendicularly oriented along the rubbing direction. Second, the BTPD-FDA PI with the relatively lowest T_g exhibits the largest surface roughness for the rubbed film. Finally, the BBBPAn-FDA PI with the largest chain rigidity and the highest T_g also shows the second largest surface roughness for the rubbed film. Here it is noted that the BBBPAn-FDA PI is composed of twisted biphenyl moieties in addition to trifluoromethyl groups.

Rubbing-Induced Molecular Orientation. To obtain information about the optical properties of the polymer chains in the rubbed PI films, an optical phase retardation technique was used. Figure 4 displays polar diagrams of the variations of the transmitted light intensity [= (in-plane birefringence) × (phase)] with the angle of rotation of the PI

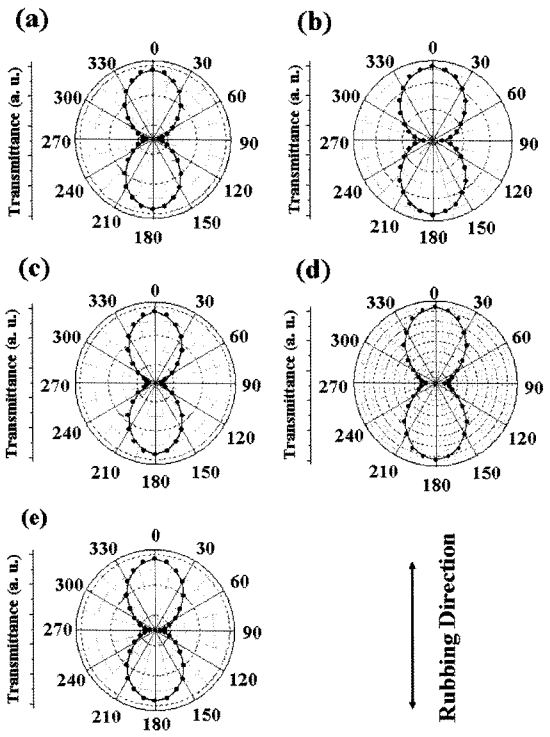

Figure 4. Polar diagrams of the variation of the retardation with the angle of rotation of the film, obtained from optical phase retardation measurements of PI films rubbed at a rubbing strength of 120 cm: (a) BBPD-ODA PI; (b) BBPD-MDA PI; (c) BBPD-FDA PI; (d) BTPD-FDA PI; (e) BBBAn-FDA PI. The arrow in the AFM image shows the rubbing direction.

films rubbed at a rubbing density of 120. As can be seen in Figure 4(a), for the rubbed BBPD-ODA film the maximum transmitted light intensity arises for the direction 0°↔180°, which is parallel to the rubbing direction, and the minimum light intensity arises for the direction 90°↔270°, which is perpendicular to the rubbing direction. Thus Figure 4(a) indicates that the polymer main chains are aligned parallel to the rubbing direction on the rubbed BBPD-ODA film.

For the rubbed BBPD-MDA film, the maximum intensity of transmitted light also arises for the direction 0°↔180°, and the minimum light intensity also arises for the direction 270°↔90° (Figure 4(b)). Thus the anisotropic polar diagram indicates that for the rubbed BBPD-MDA film the polymer main chains are aligned along the rubbing direction, and that the refractive index in the direction along the polymer main chains is higher than in the direction orthogonal to the polymer main chains, *i.e.*, these two PIs are positive birefringent polymers.

Similarly, the maximum intensity of transmitted light for the rubbed BBPD-FDA, BTPD-FDA, and BBBPAn-FDA films with bulky CF_3 groups in the repeat units also arise for the direction 0°↔180°, with the minimum light intensity in the direction 270°↔90° (Figures 4(c), (d), and (e)). Thus these anisotropic polar diagrams indicate that the polymer main chains of these three PI films are aligned along the rubbing direction, and the refractive indexes in the directions along the polymer main chains are also higher than in the directions orthogonal to the polymer main chains, *i.e.*, these PIs are also positive birefringent polymers.

Figure 5 shows the variations with rubbing strength of the in-plane birefringence Δ_{xy} of the PI films. The magnitude of Δ_{xy} increases most rapidly with rubbing strength for the rubbed BBPD-MDA film, and then levels off with further increases in the rubbing strength.

For the BBPD-ODA film, Δ_{xy} rapidly increases with rubbing strength up to 120 cm, and then levels off with further increases in the rubbing strength. Overall, the absolute value of Δ_{xy} is slightly larger for BBPD-ODA than for BBPD-MDA when their films are rubbed at the same rubbing strength. In particular, the kinked structure of the polymer repeat unit of BBPD-ODA that results from its oxygen lone pairs contributes negatively to the polymer chain alignment. Thus, the optical retardation results indicate that the polymer chain alignability of the BBPD-ODA PI along its long axis is lower than that of the BBPD-MDA PI.

For the BBPD-FDA PI film, Δ_{xy} rapidly increases with rubbing strength up to 120 cm, and then levels off with further increases in the rubbing strength. Overall, the absolute value of Δ_{xy} is smaller for the rubbed BBPD-ODA and BBPD-MDA PI films when they are rubbed at the same rubbing strength. Similar results were observed for the BTPD-FDA and BBBPAn-FDA PIs, with the ordering of the value of the in-plane birefringence (Δ_{xy}) as follows: BBPD-MDA PI > BBPD-ODA PI > BBPD-FDA PI > BTPD-FDA PI >

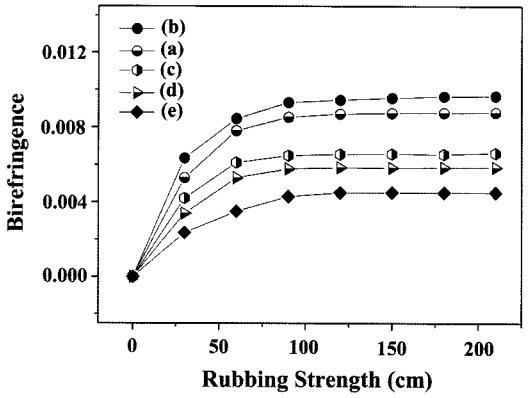

Figure 5. Variations with rubbing strength of the in-plane birefringence Δ_{xy} of the rubbed PI films: (a) BBPD-ODA PI; (b) BBPD-MDA PI; (c) BBPD-FDA PI; (d) BTPD-FDA PI; (e) BBBAn-FDA PI.

BBBPAn-FDA PI, as shown in Figure 5.

Taking into account the chemical structures of the PIs in Figure 1, the CF_3 groups in the BBPD-FDA, BTPD-FDA, and BBBPAn-FDA PIs are bulkier than the methylene groups and oxygen atoms in the BBPD-MDA and BBPD-ODA PI. This bulky group contributes negatively to the alignability of the polymer chains by causing kinked polymer chain alignment and loose packing. Note also that the BTPD-FDA PI contains bulky and flexible trimethylsilylphenyl groups, which further reduce the polymer chain interaction and rigidity, and so it has a lower value of Δ_{xy} than that of the BBPD-MDA PI; moreover the bulky and twisted biphenyl repeat structure of BBBPAn-FDA means that it has the lowest value of Δ_{xy}. Thus the differences in the variations of the in-plane birefringence Δ_{xy} with rubbing strength are due to the variation in the chemical components of the polymer repeat units.

LC Alignment and Anchoring Energy. Figure 6 shows polar diagrams of the absorbances of LC cells fabricated with PI films rubbed at a rubbing strength of 120 cm. As is clear from Figure 6(a), the LC cell of the rubbed BBPD-ODA film exhibits maximum absorbance along the direction 0° ↔180°, which is parallel to the rubbing direction. The anisotropy of this polar diagram indicates that the LC molecules in contact with the rubbed BBPD-ODA film surface are induced homogeneously to align parallel to the rubbing direction.

Similarly, the LC cells of the rubbed BBPD-MDA, BBPD-FDA, BTPD-FDA, and BBBPAn-FDA films exhibit maximum absorbance along the direction 0°↔180°, which is parallel to the rubbing direction (Figures 6(b-d), and (e)). The anisotropy of these polar diagrams indicates that the LC molecules in contact with the rubbed film surfaces are induced homogeneously to align parallel to the rubbing direction. Thus the LC molecules align parallel to the polymer main chains, which are oriented along the rubbing direction.

Taking into account the surface morphologies and the orientations of the polymer chain segments described above, and this observation that the LC molecules align parallel to the rubbing direction, we conclude that the alignment of the LCs is directly induced by the microgrooves or the strong anisotropic molecular interactions with the oriented polymer main chains (both oriented parallel to the rubbing direction).

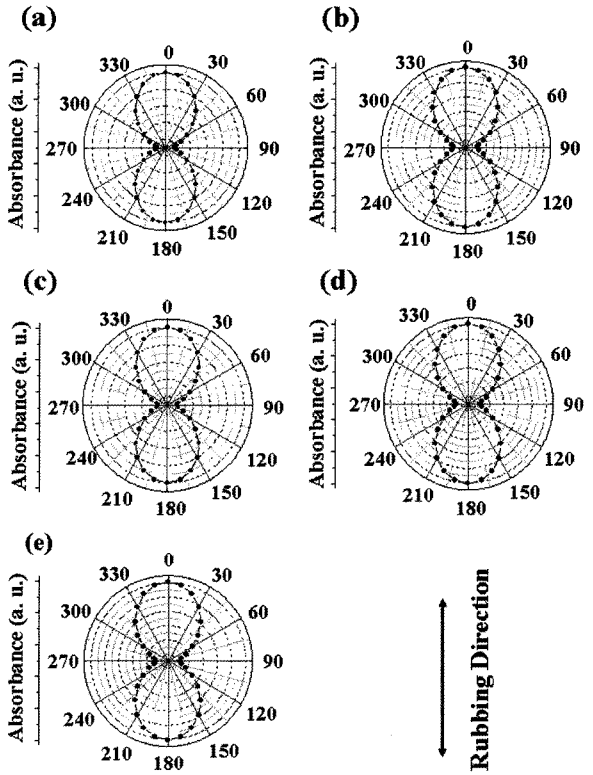

Figure 6. Polar diagrams of the light absorbance of a dichroic dye aligned with the LC molecules in antiparallel LC cells, measured as a function of the angle of rotation of each cell: (a) BBPD-ODA PI; (b) BBPD-MDA PI; (c) BBPD-FDA PI; (d) BTPD-FDA PI; (e) BBBAn-FDA PI. The PI films were rubbed at a rubbing strength of 120 cm.

The pretilt angles of the LCs in the LC cells were measured by using the crystal-rotation method. For the five LC cells fabricated with the rubbed films of the respective PIs, the measured LC pretilt angles were found to be in the range 0-1.0°, depending on the rubbing strengths employed in the rubbing process. Overall, all the PI films induce LC molecules to align with low pretilt angles on the rubbed film surfaces. In general, an LC molecule is composed of an aromatic mesogen and an aliphatic tail. The aromatic mesogen component can favorably interact with the aromatic components of an alignment layer film *via* π-π interactions, whereas the aliphatic tail can undergo van der Waals type interactions with the film's aliphatic components. It has been reported that the pretilt angles of LC molecules in contact with rubbed film surfaces are predominantly governed by the nature and length of the side groups that are oriented by

the rubbing process, and in part by the inclination of the polymer main chains oriented along the rubbing direction.[43,44,50,51,53,54,65,67,95,96]

Thus the lengths of the *t*-butylphenyl, trimethylsilylphenyl, and twisted biphenyl groups of the PIs considered here are too small to induce LC molecules to anchor with a high pretilt angle on the surfaces of the rubbed films. Furthermore, the biphenyl mesogen of the 5CB LC molecule might interact directionally and anisotropically with the parallel oriented polymer main chains, which lie in the film plane, *via* a π-π interaction, which causes the LC molecules to align with low or zero pretilt angles.

TN cells were prepared and found to be very stable and homogeneous. These TN LC cells were used in measurements of the twist angle of the LC molecules with a UV-Visible spectroscopic technique. The twist angle was measured to be 89° for the cell with a BBPD-ODA film, 89° for the cell with a BBPD-MDA film, 88° for the cell with a BBPD-FDA film, 88° for the cell with a BTPD-FDA film, and 87° for the cell with a BBBPAn-FDA film; all these PI films were rubbed with a rubbing strength of 120 cm. From the measured twist angles, the azimuthal anchoring energy of the LC molecules was determined to be 1.37×10^{-4} J/m^2 for the BBPD-ODA and BBPD-MDA PI films, 0.68×10^{-4} J/m^2 for the BBPD-FDA and BTPD-FDA PI films, and 0.45×10^{-4} J/m^2 for the BBBPAn-FDA PI film (Table II). In addition, polar anchoring energy measurements were carried out for the homogeneous anti-parallel LC cells fabricated with rubbed PI films; all the films were rubbed at a rubbing strength of 120 cm. The polar anchoring energies of the LC molecules were determined to be 4.26×10^{-5} J/m^2 for the rubbed BBPD-ODA PI film, 3.93×10^{-5} J/m^2 for the rubbed BBPD-MDA PI film, 1.24×10^{-5} J/m^2 for the rubbed BBPD-FDAPI film, 1.00×10^{-5} J/m^2 for the rubbed BTPD-FDA PI film, and 0.86×10^{-5} J/m^2 for the rubbed BBBPAn-FDA PI film. The LC anchoring energies of the rubbed PI films increase in the order BBBPAn-FDA PI < BTPD-FDA PI BBPD-FDA PI < BBPD-MDA PI BBPD-ODA PI according to the two anchoring energy measurement methods.

These results indicate that the parallel LC alignments on the rubbed PI films are very stable, and the differences between the measured anchoring energies suggest that the chemical components of the polymer chains contribute to the anchoring of the LC molecules on the rubbed film surfaces.

Table II. LC Cell Properties: Pretilt Angle, Azimuthal Anchoring Energy and Polar Anchoring Energy

Rubbed PI	Pretilt Angle (degree)	Azimuthal Anchoring Energy ($\times10^{-4}$ J/m^2)	Polar Anchoring Energy ($\times10^{-5}$ J/m^2)
TBPMDA-MDA PI	0.60	1.37	4.26
TBPMDA-ODA PI	0.62	1.37	3.93
TBPMDA-FDA	0.60	0.68	1.24
TMSPMDA-FDA	0.30	0.68	1.00
BBBPAn-FDA	0.10	0.45	0.86
SE 7492 (Nissan)	8.00	11.40	9.80

Conclusions

A series of soluble aromatic polyimides with high molecular weights were synthesized, revealing high thermal and dimensional stabilities. The WAXD analysis of the polyimides confirmed that for the BBPD-ODA, BBPD-MDA, BBPD-FDA, BTPD-FDA, and BBBPAn-FDA PIs, the incorporated bulky trifluoromethyl and twisted biphenyl substituents enhance the rigidity of the polymer chains but severely reduce the degree of space-efficient packing of the polymer chains. Similarly, the WAXD analysis found that the BBBPAn-FDA PI has the highest average *d*-spacing value, which is attributed to the bulkiness and rigidity of the twisted biphenyl groups in the polymer chains.

The surface morphologies and molecular orientations of the rubbed BBPD-ODA, BBPD-MDA, BBPD-FDA, BTPD-FDA, and BBBPAn-FDA PI films were investigated in detail by using AFM and optical retardation analysis. The LC alignment behaviors and anchoring energies of LC molecules on the rubbed films were also determined. The rubbed BBPD-ODA and BBPD-MDA PI film surfaces contain microgrooves that run in the rubbing direction, whereas the rubbed BBPD-FDA, BTPD-FDA, and BBBPAn-FDA PI film surfaces contain microgrooves that run perpendicular to the rubbing direction. The observed surface morphologies might be due to the characteristic deformation responses of the PIs to the shear force caused by the contact of fibers with the surfaces during the rubbing process. The characteristic deformation response depends on the molecular weight, rigidity, free volume, and glass transition temperature of the polymer chain, which are in turn due to the chemical components making up the polymer repeat units.

Despite the different surface morphologies of these rubbed films, the polymer main chains lie in the film plane on the surfaces of the BBPD-ODA, BBPD-MDA, BBPD-FDA, BTPD-FDA, and BBBPAn-FDA PIs, and preferentially orient along the rubbing direction. The rubbed PI film surfaces induce LC alignment parallel to the rubbing direction. The anchoring energies of these parallel LC alignments were found to be as large as those observed for conventional PI alignment layers. The differences between the anchoring energies might be due to the differences in the alignability, rigidity, efficient space packing, and interaction of the LC molecules with the chemical components of the polymer chains. In conclusion, our LC alignment, anchoring energy, surface morphology, and polymer segmental orientation results indicate that LC alignment on the surfaces of rubbed PI films is determined by the interplay between the direc-

tionally anisotropic interactions of the LC molecules with the oriented segments of the polymer main chains, and also by the chemical components of the segments of the polymer chains.

Acknowledgments. This study was supported by the Korea Science & Engineering Foundation of the Ministry of Education, Science & Technology (MEST) of Korea (National Research Lab Program and Center for Electro-Photo Behaviors in Advanced Molecular Systems) and the MEST (BK21 Program and World Class University Program). This work was also supported by the Ministry of Knowledge Economy of Korea [Display R&D Center (Grant No. F0004011-2008-31) funded under the 21st Century Frontier R&D Program].

References

(1) Y. Kim, C. S. Ha, T. Chang, W.-K. Lee, W. Goh, H. Kim, Y. Ha, and M. Ree, *J. Nanosci. Nanotechnol.*, **9**, 1533 (2009).
(2) S. G. Hahm, S. Choi, S.-H. Hong, T. J. Lee, S. Park, D. M. Kim, J. C. Kim, W.-S. Kwon, K. Kim, M.-J. Kim, O. Kim, and M. Ree, *J. Mater. Chem.*, **19**, 2207 (2009).
(3) S. G. Hahm, S. Choi, S.-H. Hong, T. J. Lee, S. Park, D. M. Kim, W.-S. Kwon, K. Kim, O. Kim, and M. Ree, *Adv. Funct. Mater.*, **18**, 3276 (2008).
(4) T. J. Shin and M. Ree, *J. Phys. Chem. B*, **111**, 13894 (2007).
(5) M. Kim, S. Choi, M. Ree, and O. Kim, *IEEE Electron Device Lett.*, **28**, 967 (2007).
(6) T. J. Shin and M. Ree, *Macromol. Chem. Phys.*, **203**, 781 (2002).
(7) M. Ree, W. H. Goh, and Y. Kim, *Polym. Bull.*, **35**, 215 (1995).
(8) M. Ree, T. J. Shin, and S. W. Lee, *Korea Polym. J.*, **9**, 1 (2001).
(9) Y. Kim, W. H. Goh, T. Chang, C. S. Ha, and M. Ree, *Adv. Eng. Mater.*, **6**, 39 (2004).
(10) T. J. Shin and M. Ree, *Langmuir*, **21**, 6081 (2005).
(11) J. Yu, M. Ree, Y. H. Park, T. J. Shin, W. Cai, D. Zhou, and K.-W. Lee, *Macromol. Chem. Phys.*, **201**, 491 (2000).
(12) S. I. Kim, M. Ree, T. J. Shin, C. Lee, T.-H. Woo, and S. B. Rhee, *Polymer*, **41**, 5173 (2000).
(13) J. Yu, M. Ree, T. J. Shin, X. Wang, W. Cai, D. Zhou, and K.-W. Lee, *J. Polym. Sci. Part B: Polym. Phys.*, **37**, 2806 (1999).
(14) S. M. Pyo, S. I. Kim, T. J. Shin, Y. H. Park, and M. Ree, *J. Polym. Sci. Part A: Polym. Chem.*, **37**, 937 (1999).
(15) Y. Kim, E. Kang, Y. S. Kwon, W. J. Cho, C. Chang, M. Ree, T. Chang, and C. S. Ha, *Synthetic Metals*, **85**, 1399 (1997).
(16) Y. Kim, W. K. Lee, W. J. Cho, C. S. Ha, M. Ree, and T. Chang, *Polym. Internl.*, **43**, 129 (1997).
(17) M. Ree, K. Kim, S. H. Woo, and H. Chang, *J. Appl. Phys.*, **81**, 698 (1997).
(18) Y. Kim, M. Ree, T. Chang, C. S. Ha, T. L. Nunes, and J. S. Lin, *J. Polym. Sci. Part B: Polym. Phys.*, **33**, 2075 (1995).
(19) M. Ree, W. H. Goh, J. W. Park, M. H. Lee, and S. B. Rhee, *Polym. Bulln.*, **35**, 129 (1995).
(20) Y. Kim, M. Ree, T. Chang, and C. S. Ha, *Polym. Bulln.*, **34**, 175 (1995).
(21) M. Ree, H. Han, and C. C. Gryte, *J. Polym. Sci. Part B: Polym. Phys.*, **33**, 505 (1995).
(22) M. Ree, K. J. Chen, and T. L. Nunes, *J. Polym. Sci. Part B: Polym. Phys.*, **33**, 453 (1995).
(23) M. Ree, T. J. Nunes, and J. S. Lin, *Polymer*, **35**, 1148 (1994).
(24) M. Ree, C. W. Chu, and M. J. Goldberg, *J. Appl. Phys.*, **75**, 1410 (1994).
(25) M. Ree, S. Swanson, and W. Volksen, *Polymer*, **34**, 1423 (1993).
(26) M. Ree, K.-R. J. Chen, and G. Czornyj, *Polym. Eng. Sci.*, **32**, 924 (1992).
(27) M. Ree, K. J. Chen, D. P. Kirby, N. Katzenellenbogen, and D. Grischkowsky, *J. Appl. Phys.*, **72**, 2014 (1992).
(28) M. Ree, T. L. Nunes, G. Czornyj, and W. Volksen, *Polymer*, **33**, 1228 (1992).
(29) M. Ree, D. Y. Yoon, and W. Volksen, *J. Polym. Sci. Part B: Polym. Phys.*, **29**, 1203 (1991).
(30) M. Ree, T. J. Shin, Y. H. Park, H. Lee, and T. Chang, *Korea Polym. J.*, **7**, 370 (1999).
(31) W. H. Goh, K. Kim, and M. Ree, *Korea Polym. J.*, **6**, 241 (1998).
(32) S. I. Kim, T. J. Shin, M. Ree, G. T. Hwang, B. H. Kim, H. Han, and J. Seo, *J. Polym. Sci. Part A: Polym. Chem.*, **37**, 2013 (1999).
(33) Y. Kim, W. H. Goh, T. Chang, C. S. Ha, and M. Ree, *Adv. Eng. Mater.*, **6**, 39 (2004).
(34) T. J. Shin, H. K. Park, S. W. Lee, B. Lee, W. Oh, J.-S. Kim, S. Baek, Y.-T. Hwang, H.-C. Kim, and M. Ree, *Polym. Eng. Sci.*, **46**, 1232 (2003).
(35) T. J. Shin, B. Lee, H. S. Youn, K.-B. Lee, and M. Ree, *Langmuir*, **17**, 7842 (2001).
(36) I. S. Chung, C. E. Park, M. Ree, and S. Y. Kim, *Chem. Mater.*, **13**, 2801 (2001).
(37) P. J. Collings and J. S. Patel, Eds., *Handbook of Liquid Crystal Research*, Oxford University Press, Oxford, 1997.
(38) J. Cognard, Eds., *Alignment of Liquid Crystals and Their Mixtures*, Gorden & Breach, London, 1982.
(39) K.-W. Lee, S.-H. Paek, A. Lien, C. During, and H. Fukuro, *Macromolecules*, **29**, 8894 (1996).
(40) N. A. J. van Aerle and J. W. Tol, *Macromolecules*, **27**, 6520 (1994).
(41) S. G. Hahm, T. J. Lee, T. Chang, J. C. Jung, W.-C. Zin, and M. Ree, *Macromolecules*, **39**, 5385 (2006).
(42) A. S. Mathews, I. Kim, and C. S. Ha, *Macromol. Res.*, **15**, 114 (2007).
(43) S. W. Kang, *Macromol. Res.*, **15**, 487 (2007).
(44) J. Y. Lee, J. H. Kim, and B. K. Rhee, *Macromol. Res.*, **15**, 234 (2007).
(45) G. Y. Lee, H. N. Jang, and W. T. Jung, *et al.*, *Macromol. Res.*, **16**, 741 (2008).
(46) S. G. Hahm, S. W. Lee, J. Suh, B. Chae, S. B. Kim, S. J. Lee, K. H. Lee, J. C. Jung, and M. Ree, *High Preform. Polym.*, **18**, 549 (2006).
(47) T. J. Lee, S. G. Hahm, S. W. Lee, B. Chae, S. J. Lee, G. Kim, S. B. Kim, J. C. Jung, and M. Ree, *Mater. Sci. Eng. B*, **132**, 64 (2006).
(48) J. K. Lee, S. J. Lee, J. C. Jung, W.-C. Zin, T. Chang, and M. Ree, *Polym. Adv. Technol.*, **17**, 444 (2006).
(49) S. B. Lee, G. J. Shin, J. H. Chi, W.-C. Zin, J. C. Jung, S. G.

Hahm, M. Ree, and T. Chang, *Poymer*, **47**, 6606 (2006).
(50) S. W. Lee, S. J. Lee, S. G. Hahm, T. J. Lee, B. Lee, B. Chae, S. B. Kim, J. C. Jung, W. C. Zin, B. H. Sohn, and M. Ree, *Macromolecules*, **38**, 4331 (2005).
(51) S. J. Lee, J. C. Jung, S. W. Lee, and M. Ree, *J. Polym. Sci. Part A: Polym. Chem.*, **42**, 3130 (2004).
(52) B. Chae, S. W. Lee, B. Lee, W. Choi, S. B. Kim, Y. M. Jung, J. C. Jung, K. H. Lee, and M. Ree, *J. Phys. Chem. B*, **107**, 11911 (2003).
(53) S. W. Lee, B. Chae, B. Lee, W. Choi, S. B. Kim, S. I. Kim, S.-M. Park, J. C. Jung, K. H. Lee, and M. Ree, *Chem. Mater.*, **15**, 3105 (2003).
(54) B. Chae, S. W. Lee, B. Lee, W. Choi, S. B. Kim, Y. M. Jung, J. C. Jung, K. H. Lee, and M. Ree, *Langmuir*, **19**, 9459 (2003).
(55) B. Chae, S. B. Kim, S. W. Lee, S. I. Kim, W. Choi, B. Lee, M. Ree, K. H. Lee, and J. C. Jung, *Macromolecules*, **35**, 10119 (2002).
(56) S. W. Lee, T. Chang, and M. Ree, *Macromol. Rapid Commun.*, **22**, 941 (2001).
(57) J. H. Park, B.-H. Sohn, J. C. Jung, S. W. Lee, and M. Ree, *J. Polym. Sci. Part B: Polym. Chem.*, **39**, 1800 (2001).
(58) J. H. Park, J. C. Jung, B. H. Sohn, S. W. Lee, and M. Ree, *J. Polym. Sci. Part A: Polym. Chem.*, **39**, 3622 (2001).
(59) S. W. Lee, S. I. Kim, Y. H. Park, M. Ree, K. H. Lee, and J. C. Jung, *Mol. Cryst. Liq. Cryst.*, **368**, 559 (2001).
(60) J. C. Jung, K. H. Lee, B. H. Sohn, S. W. Lee, and M. Ree, *Macromol. Symp.*, **164**, 227 (2001).
(61) S. W. Lee, S. I. Kim, Y. H. Park, M. Ree, Y. N. Rim, H. J. Yoon, H. C. Kim, and Y. B. Kim, *Mol. Cryst. Liq. Cryst.*, **349**, 279 (2000).
(62) S. W. Lee, S. I. Kim, Y. H. Park, M. Ree, K. H. Lee, and J. C. Jung, *Mol. Cryst. Liq. Cryst.*, **349**, 271 (2000).
(63) S. I. Kim, T. J. Shin, M. Ree, and J. C. Jung, *J. Soc. Inform. Display*, **8**, 61 (2000).
(64) M. Ree, S. I. Kim, S. M. Pyo, T. J. Shin, H. K. Park, and J. C. Jung, *Macromol. Symp.*, **142**, 73 (1999).
(65) S. I. Kim, M. Ree, T. J. Shin, and J. C. Jung, *J. Polym. Sci. Part A: Polym. Chem.*, **37**, 2909 (1999).
(66) S. I. Kim, S. M. Pyo, M. Ree, M. Park, and Y. Kim, *Mol. Cryst. Liq. Cryst.*, **316**, 209 (1998).
(67) H. Kikuchi, J. A. Logan, and D. Y. Yoon, *J. Appl. Phys.*, **79**, 6811 (1996).
(68) S. G. Hahm, T. J. Lee, and M. Ree, *Adv. Funct. Mater.*, **17**, 1359 (2007).
(69) S. G. Hahm, S. W. Lee, T. J. Lee, S. A. Cho, B. Chae, Y. M. Jung, S. B. Kim, and M. Ree, *J. Phys. Chem. B*, **112**, 4900 (2008).
(70) S. W. Lee, S. I. Kim, B. Lee, H. C. Kim, T. Chang, and M. Ree, *Langmuir*, **19**, 10381 (2003).
(71) S. W. Lee, S. I. Kim, B. Lee, W. Choi, B. Chae, S. B. Kim, and M. Ree, *Macromolecules*, **36**, 6527 (2003).
(72) M. Ree, S. I. Kim, and S. W. Lee, *Synthetic Metals*, **117**, 273 (2001).
(73) D. Kim, M. Oh-e, and Y. R. Shen, *Macromolecules*, **34**, 9125 (2001).
(74) M. G. Samant, J. Stohr, H. R. Brown, T. P. Russell, J. M. Sands, and S. K. Kumar, *Macromolecules*, **29**, 8334 (1996).
(75) M. F. Toney, T. P. Russell, J. A. Logan, H. Kikuchi, J. M. Sands, and S. K. Kumar, *Nature*, **374**, 709 (1995).
(76) K. Sakamoto, R. Arafune, N. Ito, S. Ushioda, Y. Suzuki, and S. Morokawa, *J. Appl. Phys.*, **80**, 431 (1996).
(77) D. W. Berreman, *Phys. Rev. Lett.*, **28**, 1683 (1972).
(78) P. G. de Gennes, W. Marshall, and D. H. Wilkinson, Eds., *Physics of Liquid Crystals*, Oxford, Clarendon, 1974.
(79) D. C. Flanders, D. C. Shaver, and H. I. Smith, *Appl. Phys. Lett.*, **32**, 597 (1978).
(80) A. Sugimua, N. Yamanoto, and T. Kawamura, *Jpn. J. Appl. Phys.*, **20**, 1343 (1981).
(81) M. Nakamura and M. Ura, *J. Appl. Phys.*, **52**, 210 (1981).
(82) E. S. Lee, P. Vetter, T. Miyashita, T. Uchida, M. Kano, M. Abe, and K. Sugawara, *Jpn. J. Appl. Phys.*, **32**, L1436 (1993).
(83) A. J. Pidduck, G. P. Bryan-Brown, S. Haslam, R. Bannister, I. Kitely, T. J. McMaster, and L. Boogaard, *J. Vac. Sci. Technol. A*, **14**, 1723 (1996).
(84) J. Kim and S. Kumar, *Phys. Rev. E*, **57**, 5644 (1998).
(85) M. P. Mahajan and C. Rosenblatt, *J. Appl. Phys.*, **83**, 7649 (1998).
(86) T. Uchida, M. Hirano, and H. Sakai, *Liq. Cryst.*, **5**, 1127 (1989).
(87) M. E. Becker, R. A. Killan, B. B. Kosmowski, and D. A. Mlynski, *Mol. Cryst. Liq. Cryst.*, **132**, 167 (1986).
(88) J. A. Castellano, *Mol. Cryst. Liq. Cryst.*, **94**, 33 (1983).
(89) S. W. Lee, B. Chae, S. G. Hahm, B. Lee, S. B. Kim, and M. Ree, *Polymer*, **45**, 4068 (2005).
(90) S. W. Lee and M. Ree, *J. Polym. Sci. Part B: Polym. Chem.*, **42**, 1322 (2004).
(91) B. Chae, S. W. Lee, S. B. Kim, B. Lee, and M. Ree, *Langmuir*, **19**, 6039 (2003).
(92) B. Chae, S. W. Lee, Y. M. Jung, M. Ree, and S. B. Kim, *Langmuir*, **19**, 687 (2003).
(93) B. Chae, S. W. Lee, M. Ree, and S. B. Kim, *Vibrational Spectro.*, **29**, 69 (2002).
(94) S. G. Hahm, T. J. Lee, S. W. Lee, J. Yoon, and M. Ree, *Mater. Sci. Eng. B*, **132**, 54 (2006).
(95) S. W. Lee, H. C. Kim, B. Lee, T. Chang, and M. Ree, *Macromolecules*, **36**, 9905 (2003).
(96) S. W. Lee, B. Chae, H. C. Kim, B. Lee, W. Choi, S. B. Kim, T. Chang, and M. Ree, *Langmuir*, **19**, 8735 (2003).
(97) J. C. Dubois, M. Gazard, and A. Zann, *J. Appl. Phys.*, **47**, 1270 (1975).
(98) K. Miyano, *Phys. Rev. Lett.*, **43**, 51 (1979).
(99) M. B. Feller, W. Chen, and Y. R. Shen, *Phys. Rev. A*, **43**, 6778 (1991).
(100) K. Sakamoto, R. Arafune, S. Ushioda, Y. Suzuki, and S. Morokawa, *Appl. Surf. Sci.*, **100-101**, 124 (1996).
(101) N. Mori, M. Morimoto, and K. Nakamura, *Macromolecules*, **32**, 1488 (1999).
(102) J. Stohr, M. G. Samant, J. Luning, A. C. Callegari, P. Chaudhari, J. A. Doyle, J. A. Lacey, S. A. Lien, S. Purushothaman, and J. L. Speidll, *Science*, **292**, 2299 (2001).
(103) K. Weiss, C. Woll, E. Bohm, B. Fiebranz, G. Forstmann, B. Peng, V. Scheumann, and D. Johannsmann, *Macromolecules*, **31**, 1930 (1998).
(104) J. J. Ge, C. Y. Li, G. Xue, I. K. Mann, D. Zhang, S.-Y. Wang, F. W. Harris, S. Z. D. Cheng, S.-C. Hong, X. Zhuang, and Y. R. Shen, *J. Am. Chem. Soc.*, **123**, 5768 (2001).
(105) D. Johannsmann, H. Zhou, P. Sonderkaer, H. Wierenga, B. O. Myrvold, and Y. R. Shen, *Phys. Rev. E*, **48**, 1889 (1993).

(106) G. Durand, *Physica A*, **163**, 94 (1990).
(107) V. G. Nazarenko and O. D. Lavrentovich, *Phys. Rev. E*, **49**, R990 (1994).
(108) G. Barbero, L. R. Evangelista, and N. V. Madhusudana, *Eur. Phys. J.*, **1**, 327 (1998).
(109) H.-S. Kim, Y.-H. Kim, S.-K. Ahn, and S.-K. Kwon, *Macromolecules*, **36**, 2327 (2003).
(110) Y.-H. Kim, S.-K. Ahn, H. S. Kim, and S.-K. Kwon, *J. Polym. Sci. Part A: Polym. Chem.*, **40**, 4288 (2002).
(111) Y. A. Nastishin, R. D. Polak, S. V. Ahiyanovski, V. H. Bodnar, and O. D. Lavrentovich, *J. Appl. Phys.*, **86**, 4199 (1999).
(112) X. Nie, Y.-H. Lin, T. X. Wu, H. Wang, Z. Ge, and S.-T. Wu, *J. Appl. Phys.*, **98**, 013156 (2005).
(113) M. Born and E. Wolf, Eds., *Principle of Optics*, Pergamon, Oxford, 1980.
(114) R. A. Chipman, Eds., *Handbook of Optics II*, McGraw-Hill, New York, 1995.
(115) J. M. Geary, J. W. Goodby, A. R. Kmetz, and J. S. Patel, *J. Appl. Phys.*, **62**, 4100 (1987).
(116) B. S Ban, Y. N. Rim, and Y. B. Kim, *Liq. Cryst.*, **27**, 125 (2000).
(117) Y. B. Kim and B. S. Ban, *Liq. Cryst.*, **26**, 1579 (1999).